Applied Geochemistry 116 (2020) 104564

Contents lists available at ScienceDirect

Applied Geochemistry

journal homepage: http://www.elsevier.com/locate/apgeochem

# Groundwater mixing in a heterogeneous multilayer aquifer driven by geogenic $CO_2$ fluxes: Evidence from chemical and isotopic composition of *Ferrarelle* waters (Riardo Plain, southern Italy)

Emilio Cuoco [a,*], Elisa Sacchi [b], Stefano De Francesco [a], Vittorio Paolucci [c], Erica L. Maletic [d], Thomas H. Darrah [d,e], Maurizio Sirna [a], Dario Tedesco [a,f]

[a] Department of Environmental, Biological and Pharmaceutical Sciences and Technologies, University of Campania "L. Vanvitelli", Via Vivaldi 43, 81100, Caserta, Italy
[b] Department of Earth and Environmental Sciences, University of Pavia, Via Ferrata 1, 27100, Pavia, Italy
[c] Ferrarelle S.p.A., Contrada Ferrarelle, Riardo, Italy
[d] School of Earth Sciences, The Ohio State University, 125 South Oval Mall, Columbus, OH, 43210, USA
[e] Global Water Institute, 190 North Oval Mall, Columbus, OH, 43210, USA
[f] National Institute of Geophysics and Volcanology, Osservatorio Vesuviano, Via Diocleziano 328, 80124 Napoli, Italy

ARTICLE INFO

Editorial handling by Dr D. Wolff-Boenisch

*Keywords:*
$CO_2$-saturated groundwater
Mixing geochemical tracers
$CO_2$ storage
Riardo mineral waters

ABSTRACT

The successful management of carbon in the Earth's crust is critical for mitigating the increase of anthropogenic $CO_2$ in the atmosphere. Carbon Capture and Storage (CCS) requires an understanding of the behavior of carbon in the crust and the development of robust monitoring techniques to constrain the movement, mechanisms, and pathways for any potential $CO_2$ leakage. Here, we examine an aquifer from the Riardo Plain (Campania Region, southern Italy), which serves as a suitable natural analogue for $CO_2$ migration to the critical zone (i.e., shallow crust and aquifers) and as a case study to evaluate the geochemical processes that occur when $CO_2$-saturated fluids mix with freshwater in shallow aquifers. We investigate the behavior of various geochemical constituents (major and trace elements, $\delta^{18}O$–$H_2O$, $\delta^{13}C$-DIC, and Rn content). Water from this area has a high degree of mineralization (EC 2500–3000 μS/cm), high $HCO_3^-$ (~2.5 g/L), is saturated with respect to $CaCO_3$, and is enriched in alkali ions (e.g., $Na^+ + K^+$). The high degree of mineralization occurs in groundwater that discharges from the basal aquifer of the Roccamonfina volcanic edifice (~6 km NW), with vast $CO_2$ inputs that promote host rock leaching. Superficial volcanic aquifers are recharged by fresh meteoric precipitation when groundwater flows from carbonates at the edge of the plain to aquifers hosted in the southeastern slope of the Roccamonfina volcano. The presence of normal faults in this area permits natural upwelling of $CO_2$-rich groundwater, which locally mixes with shallow freshwater present within the upper volcanic succession. Significant ($R > 0.8$) linear correlations between conservative elements suggest that groundwater geochemistry is dominated by a mixture of two main endmembers: (i) deep/mineralized waters and (ii) shallow/diluted waters. The intrusion of freshwater to volcanic aquifers induces oxidation, leading to adsorption of select elements (e.g., As and Ba) onto Fe-oxyhydroxide precipitates within these aquifers. Geochemical modeling suggests that $CO_2$ saturation approaches 3 g/L, which agrees with direct measurements of $CO_2$ flux. We conclude that our conceptual geochemical model helps to constrain mixing of $CO_2$ with freshwater and to diagnose the secondary geochemical processes that influence aqueous geochemistry within $CO_2$-influenced groundwater.

## 1. Introduction

Carbon Capture and Storage (CCS) is a technology used to remove atmospheric $CO_2$ from the atmosphere and store it for geologic time scales in order to help mitigate increasing atmospheric $CO_2$ concentrations caused by anthropogenic utilization of fossil fuels (Shaffer, 2010; Szulczewski et al., 2012). Subsurface storage is one potential mechanism of CCS, which requires an accurate characterization of the subsurface processes that confine $CO_2$ and associated brines as well as a suite of techniques that can be used to interrogate the

* Corresponding author.
*E-mail address:* emilio.cuoco@unicampania.it (E. Cuoco).

https://doi.org/10.1016/j.apgeochem.2020.104564
Received 7 May 2019; Received in revised form 14 February 2020; Accepted 27 February 2020
Available online 3 March 2020

environmental integrity of subsurface storage. For example, although highly unlikely, if $CO_2$ were to leak from the designated reservoir formation, it could change natural pressure gradients and induce mixing of $CO_2$-saturated fluids from different sources. This leakage could transport $CO_2$-saturated fluids to shallow aquifer and potentially result in noticeable changes in the chemical and isotopic composition of the mixed fluids, including shallow groundwater.

The Riardo Plain is a multi-layer aquifer located in the Campania Region of southern Italy. This study area is a suitable natural field laboratory to study groundwater mixing dynamics, specifically as it relates to the introduction of $CO_2$. The alkali- and quartz-rich volcanic succession of the Riardo Plain is a shallow and minimally mineralized aquifer that overlies the carbonate basement (Cuoco et al., 2010; Mazza et al., 2013). The deeper carbonate basement is karstic and saturated with respect to $CO_2$, resulting in a carbonate aquifer that is a source of highly mineralized and gas-rich (mainly $CO_2$) groundwater in this region (Minissale, 2004; Giordano et al., 1995). When the partial pressure of gases ($CO_2$) exceeds hydrostatic pressure, deep fluids migrate up to the surface along normal faults that serve as vertical conduits for the transport of both $CO_2$ gas and highly mineralized waters (Giordano et al., 1995). This process produces a vertical concentration gradient of dissolved gases and ions, stratifying the composition of groundwater and its geochemical reactivity within this region (Cuoco et al., 2010, 2015; Viaroli et al., 2018).

Historically, groundwater from the Riardo Plain has been exploited as an economic source of sparkling water. Since 1893 the region has been home to Ferrarelle™, which is one of the leading Italian producers of bottled water. Ferrarelle™ has drilled dozens of sparkling-water supply wells at varying discrete depths, which are extensively monitored for water quality. Hence, we refer to samples collected from these aquifer units as the "Ferrarelle system".

Here, we focus on understanding the transport, mixing, and reactivity of crustal fluids, including highly reactive $CO_2$. As part of this study, we determined the abundance of major elements, trace elements, and radon (Rn) and the isotopic compositions of water ($\delta^{18}O$–$H_2O$) and dissolved inorganic carbon ($\delta^{13}C$-DIC) in water samples collected from supply wells at varying depths. These measurements allow us to investigate their geochemical behavior along vertical flow paths. We then use geochemical data to: a) develop conceptual geochemical models to estimate the flux of $CO_2$ and other dissolved phases; b) obtain information about the flow dynamics in hydrogeological system(s); c) improve our understanding of how mixing between $CO_2$-saturated fluids and freshwater influence groundwater geochemistry; and d) provide a geochemical framework that documents the processes that would likely occur in a scenario in which $CO_2$ leaked from a CCS reservoir (e.g., Kharaka et al., 2009, 2006; Lawter et al., 2018; Nisi et al., 2019; Siller et al., 2018; Takaya et al., 2018; Xu et al., 2010; Amonette et al., 2019).

## 2. Geological and hydrogeological setting

The Ferrarelle system is located at the southwest corner of the Riardo Plain, between the Roccamonfina volcanic edifice and the Mt. Maggiore carbonate platform (Fig. 1a). The regional stratigraphy has been described previously (Giordano et al., 1995). Briefly, the basement consists of a Meso-Cenozoic carbonate succession that is dominantly dolomitic-limestone at depth and transitions to marine limestone at the top (the latter sequence is known as the Simbruini-Matese unit from Patacca and Scandone, 2007). The carbonate basement under the Ferrarelle area is highly deformed by a series of horst/graben systems, which have been buried by interbedded sequences of younger volcanoclastic deposits and spatter cones (Giordano et al., 1995). The Roccamonfina volcano was active from 550 to 150 kyr BP (Rouchon et al., 2008). This activity buried the carbonate basement with these younger successions of volcanoclastic deposits. Locally, the thickness of the volcanic deposits varies between 100 and 140 m in thickness.

The Roccamonfina volcanic field was emplaced during three main stages (De Rita and Giordano, 1996). The first stage of volcanism included effusive aphyric volcanites with high contents of lithophile elements (Wendlandt and Eggler, 1980). The second stage consisted of explosive products, including the Brown Leucitic Tuff (Luhr and Giannetti, 1987) and the White Trachytic Tuff (Giannetti and Luhr, 1983), were the main Roccamonfina volcanic products that reached the Riardo Plain. The third and final stage of volcanic activity consisted of latitic domes, which were restricted to the caldera summit (Giannetti, 2001). The Campanian Ignimbrite, which was produced by explosive activity of the Campi Flegrei 39 kyr BP, covered the Roccamonfina volcanics with 10–20 m of volcanic products (De Vivo et al., 2001).

Previous work (Cuoco et al., 2010; Minissale et al., 2004; Giordano et al., 1995) suggests that groundwater from limestone aquifer in the current study area are super-saturated with respect to $CO_2$ and are highly mineralized. The geochemistry of groundwater in the region is dominated by water-rock interactions with volcanics and limestone (Busico et al., 2018). Because of this, Cuoco et al. (2010) inferred that the carbonate aquifers in the Riardo Plain accessed by Ferrarelle™ were likely recharged near the Roccamonfina volcanic edifice. The model of recharge has been recently revised by , Viaroli et al. (2016, 2018, 2019) and considers two different groundwater flow processes, including: (a) shallow groundwater that flows along the southeast slope of the volcanic edifice towards shallow aquifers of the Riardo Plain and (b) a deeper groundwater circulation in the basal aquifer of the volcano, which recharges into the deep carbonate basement of the Riardo Plain.

## 3. Materials and methods

Thirty-three groundwater samples were collected during the summer of 2007 from active water supply wells in the Riardo Plain (Fig. 1) from two main areas: 1) the Ferrarelle system and 2) the Valdassano area. We also collected three spring samples along the southeast slope of the volcanic edifice in the Teano area. We acknowledge that these three springs do not constitute a comprehensive collection of regional spring samples. However, we suggest that the *Teano* samples provide a basis for comparison to water samples with extensive volcanic interaction, low $CO_2$, and low electrical conductivity as waters with this composition are not observed in the Ferrarelle area.

Groundwater samples were obtained from water supply wells directly at the well head by connecting the tap to the pumping device using well-accepted practices (Darrah et al., 2015; Eymold et al., 2018; Harkness et al., 2018; Kreuzer et al., 2018). All water supply wells that were actively being used by Ferrarelle™ were sampled after adequately purging sampling equipment. Water wells that were not actively being used by Ferrarelle™ were purged more than three well volumes (for approximately 2 h) or until all field parameters were verified as stable following standard protocols (USGS, 2011). Field parameters, including temperature, pH, and electric conductivity (EC, automatic compensation to 25 °C) were measured in the field using a WTW pH/cond 340i portable multiprobes. Redox potential was measured with a Hanna HI991002 portable potentiometer equipped with HI1297 probe, and detected values were subsequently converted to Eh following previous methods (Ryan, 2014).

After all field parameters were recorded, water samples were collected using a polyurethane beaker that was pre-washed with ultrapure water (18.2 MΩ resistivity) and pre-rinsed three times with sampling water. Samples were then filtered using a sterile 0.45 μm pore size cellulose acetate filter (Millipore™) following previous methods (Cuoco et al., 2013). Three sample aliquots were separated in the field, including sample aliquots collected and stored: 1) directly in polyurethane bottles without treatment, 2) in pre-acid washed polyurethane bottles that were acidified with a few drops of ultrapure $HNO_3$, and 3) in pre-acid washed polyurethane bottles that were acidified to 1% $HNO_3$ by volume. The $HCO_3^-$ concentration was quantified in the field by volumetric titration with standardized 0.1 M HCl and using methyl orange as the indicator.

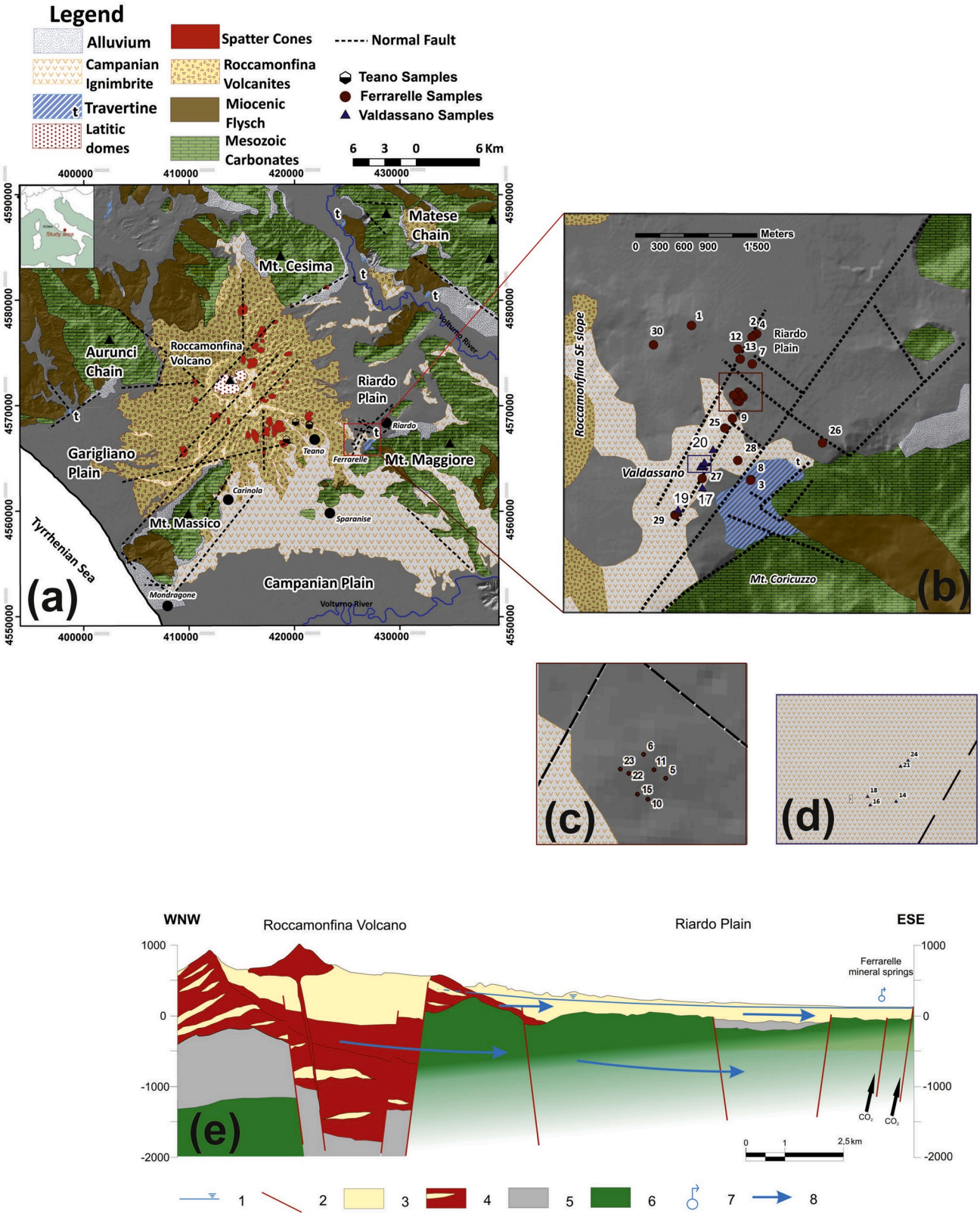


**Fig. 1. - (a)** Geological setting of the area that encompasses the Ferrarelle aquifer (square inset in the map). The surface geology of the study area and sample locations in relation to normal faults. For clarity, the Alluvium is from the Quaternary, the Campanian Ignimbrite, Latitic Domes, Roccamonfina Volcanites, and Spatter Cones are Pleistocene in age, the Miocenic Flysch is from the Miocene, and the Mesozoic carbonates are from the Mesozoic; **(b)** a zoomed in view of the study area, including Ferrarelle and Valdassano; **(c)** zoomed in sparkling-water supply well locations for Ferrarelle™; **(d)** zoomed in water supply wells locations in the Valdassano region. Note the normal faults throughout the region, which have been associated with surface expressions of sparkling $CO_2$-rich waters; and **(e)** schematic hydrogeological cross section of the Ferrarelle hydrogeological system reproduced from Viaroli et al. (2018). The cross section includes: 1) the basal aquifer water level; 2) normal fault locations; 3) pyroclastic deposits; 4) volcanoclastic deposits; 5) flysch deposits; 6) limestone units; 7) spring locations; 8) groundwater flow direction indicators.

Major elements were analyzed by ion chromatography (Dionex™ DX-120) at the Department of Environmental, Biological, and Pharmaceutical Sciences and Technologies (DISTABIF) at the University of Campania (Caserta, Italy) using either unacidified ($F^-$, $Cl^-$, $NO_3^-$, and $SO_4^{2-}$) or acidified ($Na^+$, $K^+$, $Mg^{2+}$, and $Ca^{2+}$) samples following EPA methods 300.1 and 300.7. Charge imbalances were less than ±3% (calculated using the PHREEQC computer code following Parkhurst and Appelo, 1999). Precision and accuracy for the IC analyses was tested by measuring certificated reference materials, confirming uncertainties better than 7% errors.

Trace elements were analyzed by inductively-coupled plasma mass spectrometry (Agilent™ 7500ce) equipped with a collision cell designed to eliminate polyatomic interferences (Octopole Reaction System (ORS) Technology) at DISTABIF following methods reported in Cuoco et al. (2013). Instrumental drift was monitored continuously using an $^{89}Y$–$^{159}Tb$ internal standard with known concentration. The analytical precision and accuracy were determined by repeated quantifications of Agilent™ certified solution and were better than 10%.

Samples for $\delta^{13}$C-DIC analyses were pretreated to precipitate carbonates as $SrCO_3$ and then dried in a controlled atmosphere in order to avoid contamination by atmospheric $CO_2$. The precipitate was digested with orthophosphoric acid and the $CO_2$ that evolved from that reaction was analyzed using a Finnigan™ MAT 250 isotope ratio mass spectrometer (IRMS). The analytical error for $\delta^{13}$C-DIC measurements was ±0.2‰ and results were expressed relative to the international standard V-PDB. Oxygen isotopes were analyzed using the $CO_2$–$H_2O$ equilibration method proposed by Epstein and Mayeda (1953) using a Finnigan™ MAT 250 IRMS. The experimental error for $\delta^2H$–$H_2O$ was ±0.2‰ as determined by internal standards that were previously calibrated relative to the international standard V-SMOW.

The $^{222}$Rn concentrations were measured from samples collected in 250 mL polyurethane bottles filled without headspace, under water surface and then immediately sealed avoiding loss of radon by degassing. Radon concentrations were determined using a Rad7 radon detector purchased from Durridge™ following the method of De Francesco et al. (2010b). The accuracy for $^{222}$Rn was better than 5%.

Dissolved ionic speciation calculations, saturation indices (SI) and geochemical modeling were performed using the PHREEQC code and database (Parkhurst and Appelo, 1999) through its interactive interface PhreeqcI v. 3.4.0.12927.

## 4. Results

### 4.1. Chemical parameters

The results of all geochemical analyses are reported in Table 1. The hydrogeochemical types of waters from the study area are shown in the Piper diagram in Fig. 2. To better recognize the geochemical processes involved, *Ferrarelle*, *Valdassano*, and *Teano* samples were demarcated using different symbols. All samples are Ca–$HCO_3$ type waters with a high predominance of dissolved $CaCO_3$, with the exception of the *Teano* samples and one *Ferrarelle* sample (sample #1) (Fig. 2). Sample #1 shows the characteristic hydrogeochemical type of shallow Roccamonfina aquifers (Cuoco et al., 2010) and is similar to the unpolluted *Teano* sample (T3). The remaining *Teano* samples (T1 and T2) exhibit contamination of $NO_3^-$ (78–109 mg/L) and $SO_4^{2-}$ (35–38 mg/L) already documented as related to agricultural pollution (Cuoco et al., 2015).

In order to investigate the behavior of chemical variables in the current dataset, a correlation matrix was computed (Table 2). Fig. 3 illustrates the strong linear relationship (R = 0.99; N = 30; p < 0.01) between $HCO_3^-$ and electric conductivity (EC). Notably, as salinity increases (EC 2000–3300 μS/Cm), the $HCO_3^-$ also increases (1500–2900 mg/L).

The relative percentages of total cations in solution ($\frac{Na+K}{\Sigma Cations} \times 100$) (calculated from concentrations expressed in meq/L) decrease with increasing $HCO_3^-$ content (Fig. 4a). The *Ferrarelle* samples with the highest proportion of alkali ion content (with $([Na^+] + [K^+])$ of greater than 25% of the total metals; #1 and #2) displayed the lowest degree of mineralization (EC < 625 μS/cm) as well as the lowest $HCO_3^-$ content (<500 mg/L) (Fig. 4a). Conversely, samples with the highest absolute concentrations of both alkali ions, but lowest proportions of alkali ions in the total metal content are the most saline and gas-saturated waters in the study area (EC > 3,000 μS/cm; $HCO_3^-$ ~2800 mg/L; #28-#30); each of these samples are saturated with respect to $CaCO_3$ ($SI_{CaCO3} > 0$, Table 1). Therefore, we suggest that although samples with high degrees of mineralization display high levels of alkali ions, highly mineralized waters actually display the lowest relative percentage of these elements.

The alkali and alkali-earth metals (both major and minor elements), B, and $Cl^-$ show high correlations with each other (0.60 < R < 0.99; p < 0.05) (see Table 2). In most cases, Eh values vary inversely with the amounts of redox-sensitive elements (Mn, Fe, and As). In fact, the concentration of these three elements show an inverse correlation with Eh (R = −0.67, −0.86, and −0.57, respectively, with a p < 0.05) (Table 2). Finally, the highly mineralized waters (EC > 2700 μS/cm), with the highest $HCO_3^-$ and $CO_2$ gas content show the highest concentration of conservative ions and redox sensitive elements.

To gain further insight into the processes that influence the geochemistry of waters that display low to medium levels of mineralization, we plot [Sr] vs. [Ba] (Fig. 5a). These results highlight two different trends. Trend A includes the *Ferrarelle* waters and displays a well-correlated ([Ba] = 0.14[Sr] −3.19; R = 0.95; N = 19; p < 0.01). Trend A samples also show a strong enrichment of [Ba] with increasing $CaCO_3$ saturation index (Fig. 5b). By comparison, Trend B includes *Valdassano* waters and shows a weak correlation between Ba and Sr ([Ba] = 0.01[Sr] + 7.40; R = 0.62; N = 8; p = 0.07) and does not display a concordant increase in Ba with Sr. Trend B waters show a significant correlation between [Ba] and $CaCO_3$ saturation index, but do not exhibit the same degree of Ba enrichment as observed in Trend A.

The highest concentrations of $NO_3^-$, $SO_4^{2-}$, and V were always detected in samples from shallow aquifers waters with low degrees of mineralization (5–12 mg/L, 4–10 mg/L, and 5–25 μg/L respectively), whereas deep and mineralized waters always show significantly lower $NO_3^-$, $SO_4^{2-}$, and V concentrations. Negative correlations with conservative ions are similar to this trend (see Table 2).

### 4.2. Dissolved gases and isotopic markers

Groundwater samples from the study area are dominated by $CO_2$, which accounts for ~99% of the dissolved gas in our study area (Cuoco et al., 2017; Minissale, 2004). The $[HCO_3^-]$ in solution is dependent on $P_{CO2}$ (e.g., Stumm and Morgan, 1996; Drever, 1997; Langmuir, 1997). Fig. 6a shows the strong linear correlation (R = 0.99) between $[HCO_3^-]$ and $\delta^{13}$C-DIC. Along this trend, the most mineralized samples ($HCO_3^-$ >2,000 mg/L; #26, #28 Fig. 6a) display the most enriched $\delta^{13}$C-DIC values (between −2 and 4‰). Samples with a higher degree of mineralization (#28, #30) show a $\delta^{13}$C-DIC composition of ~4‰, which is assumed to be the isotopic composition of the dissolved $CO_2$ hosted in the karst aquifer. Along this trend, the $\delta^{13}$C-DIC values gradually became more negative with increasing contributions of shallow groundwater. However, six samples with low relatively low degrees of mineralization appear to diverge from this trend (highlighted by trend 'A' in Fig. 6a).

$HCO_3^-$ shows a significant correlation $\delta^{18}O$–$H_2O$ (R = −0.68, p < 0.01, Table 2) with the more enriched $\delta^{18}O$–$H_2O$ values corresponding to the lowest $HCO_3^-$ concentrations (Fig. 6b). However, for samples with $HCO_3^-$ concentrations lower than 1,000 mg/L, $\delta^{18}O$–$H_2O$ values follow a secondary sub-trend that include the *Ferrarelle* samples with a low degree of mineralization (#1, #2, #5, #7, #9, #10, #11) and samples from the *Teano* area (Fig. 6b). Similar to $HCO_3^-$ concentrations, the inverse relationship between $\delta^{18}O$–$H_2O$ and $\delta^{13}$C-DIC (Fig. 6c) also exhibits significant linear correlations (R = −0.74; N = 13; p < 0.01)

**Table 1**
- Chemical, isotopic and Rn composition data of sampled groundwater. na = not analyzed.

| ID | note | depth | T | pH | EC | Eh | $HCO_3$ | $F^-$ | $Cl^-$ | $NO_3$ | $SO_4^{2-}$ | $Na^+$ | $K^+$ | $Mg^{2+}$ | $Ca^{2+}$ | Li | B | V | Mn | Fe | As | Sr | Cs | Ba | Rn | $\delta^{18}O$-$H_2O$ | $\delta^{13}C$-DIC | SI $CaCO_3$ |
|---|---|---|---|---|---|---|---|---|---|---|---|---|---|---|---|---|---|---|---|---|---|---|---|---|---|---|---|---|
| | | m | °C | | μS/cm | mV | mg/L | mg/L | mg/L | mg/L | mg/L | mg/L | mg/L | mg/L | mg/L | μg/L | μg/L | μg/L | μg/L | μg/L | μg/L | μg/L | μg/L | μg/L | μg/L | Bq/L | ‰ SMOW | ‰ PDB | |
| **#1** | *ferrarelle* | 60 | 17 | 6.3 | 383 | 208 | 201.2 | 1.1 | 15.4 | 9.5 | 4 | 32 | 28.8 | 4.6 | 30.5 | 28 | 93 | 13 | <1 | 4 | 5 | 101 | 10 | 6 | 80 | -6.4 | na | -1.01 |
| **#2** | *ferrarelle* | 60 | 20 | 7.5 | 625 | 138 | 351.4 | 1.2 | 13.5 | 10.1 | 4.7 | 25.4 | 20.9 | 3.4 | 82.4 | 25 | 63 | 18 | <1 | 4 | 8 | 136 | 14 | 7 | 10 | -6.2 | na | 0.44 |
| **#3** | *ferrarelle* | 44 | 18 | 7 | 630 | 240 | 389.5 | 0.4 | 22.1 | 12.4 | 10.2 | 15.8 | 5.1 | 7.9 | 114.7 | na | na | na | na | na | na | na | na | na | 8 | na | na | 0.04 |
| **#4** | *ferrarelle* | 60 | 19 | 6.8 | 674 | 160 | 389.8 | 1 | 13.7 | 10 | 4.6 | 25.7 | 21.1 | 4.7 | 92.1 | 28 | 83 | 17 | <1 | 6 | 7 | 203 | 14 | 26 | 35 | na | na | -0.20 |
| **#5** | *ferrarelle* | 41 | 18 | 5.8 | 1012 | 244 | 638.6 | 0.9 | 17.1 | 10.4 | 4.1 | 39 | 32.2 | 8.3 | 159.3 | 42 | 277 | 17 | 3 | 2 | 8 | 272 | <1 | 41 | 16 | -6.1 | -1.0 | -0.80 |
| **#6** | *ferrarelle* | 42 | 19 | 6 | 1100 | 156 | 681.4 | 0.9 | 12.6 | 8.7 | 3.3 | 37.7 | 30.5 | 8.5 | 173.7 | 47 | 302 | 17 | 2 | 2 | 7 | 257 | <1 | 41 | 5 | -5.8 | -1.7 | -0.56 |
| **#7** | *ferrarelle* | 133 | 18 | 6.5 | 1040 | 240 | 713.1 | 1.2 | 13.8 | 7.1 | 4.7 | 34.8 | 30.6 | 6.8 | 190.2 | 37 | 127 | 14 | 3 | 3 | 8 | 272 | 18 | 13 | 5 | -6.2 | -0.1 | -0.03 |
| **#8** | *ferrarelle* | 74 | 18 | 6 | 1070 | 154 | 714 | 0.9 | 17.7 | 10.2 | 8.9 | 24.1 | 16.5 | 15.4 | 201.6 | na | na | na | na | na | na | na | na | na | 7 | na | na | -0.55 |
| **#9** | *ferrarelle* | 95 | 20 | 6.5 | 1233 | 175 | 787 | 1.3 | 14.5 | 8.3 | 4.3 | 30.6 | 29.7 | 9.3 | 214.2 | 45 | 187 | 6 | 1 | 21 | 14 | 356 | 25 | 32 | 5 | -6.2 | na | 0.06 |
| **#10** | *ferrarelle* | 24 | 18 | 5.8 | 1256 | 214 | 793.7 | 1.3 | 15.3 | 6.7 | 4.2 | 36.5 | 28.8 | 9.9 | 212.9 | 69 | 177 | 16 | <1 | 6 | 7 | 397 | <1 | 76 | 8 | -6.3 | -2.1 | -0.64 |
| **#11** | *ferrarelle* | 38 | 20 | 5.8 | 1250 | 171 | 806.5 | 0.5 | 14.6 | 8.2 | 3.2 | 41.8 | 35.1 | 10.9 | 212.7 | 53 | 310 | 17 | 1 | 1 | 6 | 312 | <1 | 43 | 7 | -6.3 | 0.3 | -0.66 |
| **#12** | *ferrarelle* | 145 | 18 | 6.3 | 1187 | 214 | 819.8 | 1.3 | 15.8 | 6 | 4.7 | 38 | 34.1 | 8.4 | 223.6 | 43 | 183 | 11 | 55 | 42 | 5 | 336 | 19 | 20 | 9 | -6.0 | -1.5 | -0.16 |
| **#13** | *ferrarelle* | 128 | 19 | 6.3 | 1190 | 216 | 839.2 | 1.3 | 15.3 | 6 | 4.7 | 38.3 | 34.1 | 8.2 | 230.4 | 42 | 172 | 12 | 6 | 3 | 6 | 332 | 19 | 18 | 6 | -5.9 | 0 | -0.10 |
| **#14** | *valdassano* | 18 | 18 | 5.7 | 1362 | 306 | 899.9 | 1 | 22.1 | 5.8 | 4.4 | 37.6 | 30.6 | 16.7 | 222.1 | 87 | 260 | 3 | 79 | 6 | 5 | 526 | 6 | 12 | na | -6.0 | na | -0.71 |
| **#15** | *ferrarelle* | 23 | 17 | 5.8 | 1586 | 226 | 904.1 | 1.2 | 12.6 | 7.3 | 4 | 42.7 | 33.4 | 12.7 | 229 | 74 | 315 | 18 | 3 | 3 | 7 | 402 | 4 | 69 | 17 | -6.1 | -1.6 | -0.55 |
| **#16** | *valdassano* | 18 | 18 | 5.9 | 1468 | 192 | 927.3 | 1.3 | 19.6 | 7.9 | 5.7 | 50.7 | 39 | 17.2 | 224.2 | 72 | 225 | 7 | 257 | 125 | 9 | 475 | 3 | 11 | 10 | -6.4 | na | -0.50 |
| **#17** | *valdassano* | 33 | 19 | 5.8 | 1240 | 225 | 939.5 | 0.6 | 23.5 | 12.1 | 6 | 33.5 | 24.1 | 20.4 | 256.5 | 69 | 259 | 7 | 195 | 18 | 3 | 654 | 13 | 23 | 16 | -6.3 | na | -0.51 |
| **#18** | *valdassano* | 18 | 17 | 5.7 | 1708 | 275 | 1187.1 | 1.2 | 27.6 | 10.9 | 5.4 | 53.5 | 43.7 | 21.5 | 299.9 | 73 | 338 | 10 | 4 | 9 | 12 | 617 | 3 | 10 | 11 | -6.0 | na | -0.54 |
| **#19** | *valdassano* | 51 | 18 | 5.8 | 1438 | 79 | 1221.2 | 1.2 | 20.5 | <0.1 | 5 | 63.5 | 44.4 | 22.1 | 291.5 | 85 | 366 | 1 | 851 | 5275 | 10 | 495 | <1 | na | 23 | -6.3 | na | -0.34 |
| **#20** | *valdassano* | 120 | 18 | 5.8 | 1966 | 236 | 1385.7 | 0.9 | 21.4 | 5.9 | 3 | 54.2 | 47.9 | 24.7 | 360.3 | 85 | 517 | 12 | 9 | 3 | 8 | 731 | 8 | 50 | 8 | na | 1.2 | -0.28 |
| **#21** | *valdassano* | 18 | 17 | 5.7 | 2054 | 258 | 1454.3 | 1.1 | 28.9 | 8.2 | 4.7 | 58.5 | 48.7 | 26.7 | 374.2 | 81 | 410 | 13 | 8 | 22 | 11 | 740 | 3 | 22 | 9 | -6.2 | na | -0.30 |
| **#22** | *ferrarelle* | 27 | 17 | 5.8 | 2026 | 231 | 1459.4 | 0.9 | 19.3 | 4.9 | 2.4 | 54.1 | 46.1 | 19.1 | 361 | 83 | 552 | 22 | 8 | 2 | 6 | 513 | 1 | 102 | 10 | -6.3 | 0 | -0.26 |
| **#23** | *ferrarelle* | 26 | 17 | 5.9 | 2258 | 249 | 1481.9 | 0.8 | 19.8 | 3.8 | 3.3 | 56.2 | 48.1 | 19.8 | 422.8 | 101 | 564 | 19 | 78 | 13 | 6 | 650 | 1 | 107 | 8 | -6.4 | 1.4 | -0.09 |
| **#24** | *valdassano* | 18 | 18 | 5.9 | 2323 | 205 | 1689.9 | 1.1 | 24.7 | 4.9 | 5.4 | 64 | 52.9 | 31.1 | 426.1 | 99 | 382 | 7 | 649 | 111 | 9 | 858 | 5 | 17 | 6 | -6.3 | na | -0.02 |
| **#25** | *ferrarelle* | 120 | 19 | 6 | 2812 | 66 | 1901.6 | 1.4 | 21.7 | <0.1 | 2.2 | 66.4 | 71.5 | 33.4 | 464.8 | 141 | 741 | <1 | 460 | 4646 | 25 | 1196 | 67 | 168 | 1 | -6.4 | 1.3 | 0.13 |
| **#26** | *ferrarelle* | 146 | 18 | 5.9 | 2555 | 139 | 2079 | 1.1 | 26.7 | 1.8 | 3.2 | 65.1 | 58 | 40.2 | 523.2 | 117 | 689 | 4 | 465 | 838 | 7 | 998 | 43 | 119 | 2 | -6.5 | 1.7 | 0.14 |
| **#27** | *ferrarelle* | 138 | 19 | 6.1 | 3082 | 48 | 2370.1 | 1 | 27.4 | <0.1 | 2.2 | 76.8 | 60.8 | 45.5 | 608.8 | 193 | 778 | 2 | 702 | 4617 | 9 | 1267 | 4 | 137 | 17 | -6.6 | na | 0.44 |
| **#28** | *ferrarelle* | 120 | 19 | 6.2 | 3458 | 29 | 2770.7 | 1.2 | 30.5 | <0.1 | 0.9 | 93.1 | 87.2 | 51.9 | 704.1 | 172 | 996 | <1 | 427 | 5004 | 32 | 1624 | 88 | 233 | 0.4 | -6.6 | 3.9 | 0.66 |
| **#29** | *ferrarelle* | 267 | 19 | 6.1 | 3350 | 18 | 2805.9 | 1.2 | 30.3 | <0.1 | 0.7 | 95.1 | 89.4 | 53.3 | 712.9 | 159 | 879 | <1 | 409 | 4825 | 12 | 1598 | 85 | 243 | 2 | -7 | na | 0.49 |
| **#30** | *ferrarelle* | 295 | 18 | 6 | 3269 | na | 2855 | 1 | 24 | <0.1 | 1.8 | 78.7 | 86.1 | 60.9 | 656.7 | 154 | 1106 | <1 | 732 | 3845 | 16 | 1666 | 48 | 211 | na | na | 4.1 | 0.37 |
| **#T1** | *Teano* | spring | 16 | 6.7 | 536 | na | 122 | 0.2 | 46 | 109.3 | 34.8 | 29 | 12.4 | 18.2 | 51.2 | na | na | na | na | na | na | na | na | na | na | -6.3 | na | - |
| **#T2** | *Teano* | spring | 17 | 5.8 | 385 | na | 60.4 | 0.4 | 29.7 | 78.4 | 38.4 | 26.2 | 4.7 | 10.5 | 34.4 | na | na | na | na | na | na | na | na | na | na | -6.4 | na | - |
| **#T3** | *Teano* | spring | 13 | 5.8 | 247 | na | 117.2 | 0.5 | 16 | 2.6 | 7.6 | 20.6 | 25.7 | 5.5 | 16 | na | na | na | na | na | na | na | na | na | na | -6.2 | na | - |

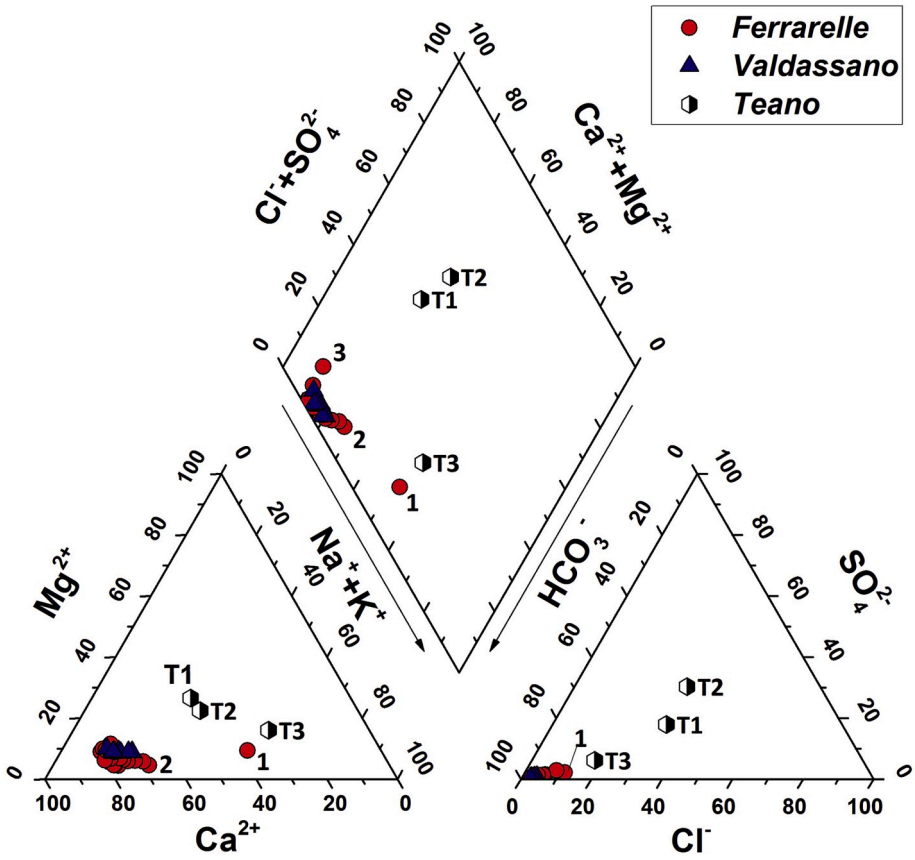


**Fig. 2.** – Piper diagram of water samples from the region. All samples are Ca–$HCO_3$ type waters with a high predominance of dissolved $CaCO_3$, with the exception of the *Teano* samples and one *Ferrarelle* sample (sample #1). Sample #1 and one of the *Teano* samples (T3) show similar geochemical types and are characteristic of the shallow Roccamonfina aquifers. The other two samples (T1 and T2) show a larger proportion of $SO_4^{2-}$ due to contamination from agricultural soil leaching.

implying a similar range of $HCO_3^-$ in each endmember.

Unlike the relatively conservative ions (Na, K, Sr), $^{222}Rn$ does not show significant correlation with $HCO_3^-$, $\delta^{13}C$-DIC, or other ionic parameters. In general, $^{222}Rn$ is highest in samples collected from the shallowest aquifers in volcanic materials (e.g., #1, 80 Bq/L) and decreases to below 5 Bq/L in the $CO_2$-gas saturated-waters.

## 5. Discussion

### 5.1. Behavior of major ions and $CO_2$

The strong linear correlations between most of the chemical variables measured in the current study are consistent with the occurrence of a dominantly two-component mixing process in the shallow aquifers, as suggested by Giordano et al. (1995) and Cuoco et al. (2010). The proposed endmembers of the mixing process are: (i) a deep, highly mineralized, and $CO_2$-rich source of water hosted in the karst aquifer in the carbonate basement and (ii) a shallowly sourced water with a relatively low degree of mineralization hosted in the multilayered strata of the volcanic successions of the Riardo Plain.

Groundwater in the deep aquifer occurs at pressures that exceed the anticipated local hydrostatic pressure gradient (Giordano et al., 1995). This over-pressured scenario likely occurs as the result of additional fluid pressure from $CO_2$ gas (Glennon and Pfaff, 2005; Lu et al., 2005). Normal faults that are present in discrete locations act as vertical conduits for fluid flow similar to those in other aquifers that are influenced by volcanic systems (Bense et al., 2013; Brunetti et al., 2013; Chen et al., 2013) (see Fig. 1); these planar discontinuities allow over-pressured fluids to flow upward and mix with freshwater hosted in shallower formations.

The mixture of a deep $CO_2$-saturated groundwater with a shallow $CO_2$-poor groundwater results in the $HCO_3^-$ concentration gradient observed in the dataset. Similarly, the extremely high correlation ($R = 0.99$) of $HCO_3^-$ with electrical conductivity (EC) can also be explained by conservative mixing between deeper $CO_2$-rich and shallower relatively freshwater endmembers (Fig. 3).

Although we cannot reliably constrain the endmembers in this system, we assume that the deeper $CO_2$-rich endmember would have a [$HCO_3^-$] that is in equilibrium with saturation conditions, suggesting that the $HCO_3$–rich endmember must be at least ten times more enriched in $HCO_3^-$ than the shallower, fresher endmember. In effect, the highly correlated mixing line records dilute of the $HCO_3$–rich endmember with freshwater that previously interacted with shallow volcanoclastic sediments. The conservative mixing ('dilution') process is recorded for $HCO_3^-$ and all measured conservative elements (e.g., Na, Cl, K, Li, B, Sr) as demonstrated by their highly significant correlations with $HCO_3^-$ (see Table 2).

It is important to note that even though the $HCO_3$–rich endmember is sourced and hosted within a carbonate aquifer, the groundwater chemistry is still heavily influenced elements likely derived from water-rock interactions with volcanic facies (e.g., F, K, Li, Rb, Fe, Mn, As) (Fig. 4). This suggests that the chemical composition of the $CO_2$-saturated groundwater hosted in the carbonate basement itself likely reflects water-rock (and potentially gas-water-rock) interactions with two different host lithologies, including: (a) volcanics found in the basal aquifer of the Roccamonfina volcano and (b) carbonates located stratigraphically below the volcanics in the Riardo Plain, prior to mixing with shallow, fresher water. The high degrees of mineralization and elevated $CO_2$ levels of the deep groundwater in the carbonate basement of the Riardo Plain area observed in this study are consistent with low-

**Table 2**
- Correlation matrix (R Pearson) for all measured parameters.

| | $T$ | $pH$ | $EC$ | $Eh$ | $HCO_3^-$ | $F^-$ | $Cl^-$ | $NO_3^-$ | $SO_4^{2-}$ | $Na^+$ | $K^+$ | $Mg^{2+}$ | $Ca^{2+}$ | $Li$ | $B$ | $V$ | $Mn$ | $Fe$ | $As$ | $Sr$ | $Cs$ | $Ba$ | $Rn$ | $\delta^{18}O$ | $\delta^{13}C$ | $IS_{CaCO3}$ |
|---|---|---|---|---|---|---|---|---|---|---|---|---|---|---|---|---|---|---|---|---|---|---|---|---|---|---|
| **T** | 1 | | | | | | | | | | | | | | | | | | | | | | | | | |
| pH | 0.46 | 1 | | | | | | | | | | | | | | | | | | | | | | | | |
| ***EC*** | −0.02 | −0.36 | 1 | | | | | | | | | | | | | | | | | | | | | | | |
| ***Eh*** | −0.56 | −0.20 | −0.54 | 1 | | | | | | | | | | | | | | | | | | | | | | |
| $HCO_3^-$ | 0.03 | −0.32 | 0.99 | −0.59 | 1 | | | | | | | | | | | | | | | | | | | | | |
| $F^-$ | −0.03 | 0.03 | 0.20 | −0.26 | 0.18 | 1 | | | | | | | | | | | | | | | | | | | | |
| $Cl^-$ | −0.05 | −0.32 | 0.75 | −0.29 | 0.77 | −0.02 | 1 | | | | | | | | | | | | | | | | | | | |
| $NO_3^-$ | 0.35 | 0.34 | −0.72 | −0.02 | −0.71 | −0.33 | −0.13 | 1 | | | | | | | | | | | | | | | | | | |
| $SO_4^{2-}$ | −0.08 | 0.24 | −0.67 | 0.46 | −0.65 | −0.32 | −0.24 | 0.59 | 1 | | | | | | | | | | | | | | | | | |
| $Na^+$ | −0.02 | −0.38 | 0.94 | −0.59 | 0.95 | 0.28 | 0.75 | −0.69 | −0.72 | 1 | | | | | | | | | | | | | | | | |
| $K^+$ | 0.01 | −0.32 | 0.95 | −0.60 | 0.95 | 0.32 | 0.68 | −0.75 | −0.78 | 0.97 | 1 | | | | | | | | | | | | | | | |
| $Mg^{2+}$ | 0.05 | −0.31 | 0.95 | −0.61 | 0.98 | 0.11 | 0.82 | −0.52 | −0.56 | 0.91 | 0.91 | 1 | | | | | | | | | | | | | | |
| $Ca^{2+}$ | 0.04 | −0.32 | 0.99 | −0.57 | 1.00 | 0.16 | 0.78 | −0.71 | −0.64 | 0.94 | 0.94 | 0.96 | 1 | | | | | | | | | | | | | |
| ***Li*** | 0.04 | −0.31 | 0.96 | −0.61 | 0.95 | 0.05 | 0.79 | −0.64 | −0.70 | 0.92 | 0.90 | 0.94 | 0.95 | 1 | | | | | | | | | | | | |
| ***B*** | −0.01 | −0.29 | 0.96 | −0.60 | 0.96 | −0.05 | 0.72 | −0.63 | −0.81 | 0.92 | 0.95 | 0.95 | 0.95 | 0.92 | 1 | | | | | | | | | | | |
| ***V*** | −0.34 | 0.15 | −0.58 | 0.57 | −0.63 | −0.35 | −0.65 | 0.13 | 0.23 | −0.62 | −0.62 | −0.71 | −0.60 | −0.66 | −0.53 | 1 | | | | | | | | | | |
| ***Mn*** | 0.19 | 0.03 | 0.63 | −0.71 | 0.69 | 0.19 | 0.52 | −0.40 | −0.28 | 0.70 | 0.64 | 0.73 | 0.65 | 0.72 | 0.61 | −0.73 | 1 | | | | | | | | | |
| ***Fe*** | 0.28 | −0.03 | 0.71 | −0.86 | 0.75 | 0.24 | 0.55 | −0.53 | −0.63 | 0.79 | 0.78 | 0.75 | 0.73 | 0.79 | 0.74 | −0.73 | 0.79 | 1 | | | | | | | | |
| ***As*** | 0.21 | 0.06 | 0.62 | −0.58 | 0.60 | 0.39 | 0.45 | 0.12 | −0.54 | 0.62 | 0.70 | 0.58 | 0.58 | 0.58 | 0.62 | −0.53 | 0.37 | 0.67 | 1 | | | | | | | |
| ***Sr*** | 0.10 | −0.24 | 0.96 | −0.62 | 0.98 | 0.08 | 0.82 | −0.52 | −0.70 | 0.93 | 0.95 | 0.98 | 0.97 | 0.95 | 0.95 | −0.71 | 0.67 | 0.77 | 0.65 | 1 | | | | | | |
| ***Cs*** | 0.44 | 0.10 | 0.61 | −0.78 | 0.65 | 0.34 | 0.41 | −0.24 | −0.71 | 0.63 | 0.74 | 0.63 | 0.64 | 0.56 | 0.65 | −0.64 | 0.46 | 0.79 | 0.75 | 0.71 | 1 | | | | | |
| ***Ba*** | 0.13 | −0.12 | 0.87 | −0.76 | 0.88 | 0.08 | 0.55 | −0.62 | −0.90 | 0.85 | 0.90 | 0.84 | 0.87 | 0.85 | 0.92 | −0.48 | 0.63 | 0.89 | 0.65 | 0.87 | 0.80 | 1 | | | | |
| ***Rn*** | −0.26 | 0.11 | −0.44 | 0.12 | −0.41 | −0.04 | −0.25 | 0.28 | 0.07 | −0.27 | −0.29 | −0.33 | −0.44 | −0.34 | −0.39 | 0.17 | 0.15 | −0.13 | −0.31 | −0.40 | −0.32 | −0.33 | 1 | | | |
| $\delta^{18}O$ | −0.22 | −0.01 | −0.68 | 0.66 | −0.72 | −0.02 | −0.58 | 0.27 | 0.60 | −0.72 | −0.73 | −0.74 | −0.71 | −0.70 | −0.69 | 0.48 | −0.59 | −0.64 | −0.35 | −0.73 | −0.60 | −0.75 | −0.01 | 1 | | |
| $\delta^{13}C$ | 0.25 | 0.15 | 0.86 | −0.60 | 0.88 | −0.06 | 0.88 | −0.65 | −0.74 | 0.89 | 0.88 | 0.87 | 0.90 | 0.80 | 0.85 | −0.64 | 0.71 | 0.68 | 0.67 | 0.86 | 0.70 | 0.73 | −0.61 | −0.76 | 1 | |
| $IS_{CaCO3}$ | 0.41 | 0.45 | 0.64 | −0.63 | 0.66 | 0.21 | 0.44 | −0.26 | −0.37 | 0.55 | 0.59 | 0.62 | 0.67 | 0.62 | 0.62 | −0.44 | 0.57 | 0.60 | 0.57 | 0.68 | 0.65 | 0.65 | −0.47 | −0.52 | 0.81 | 1 |

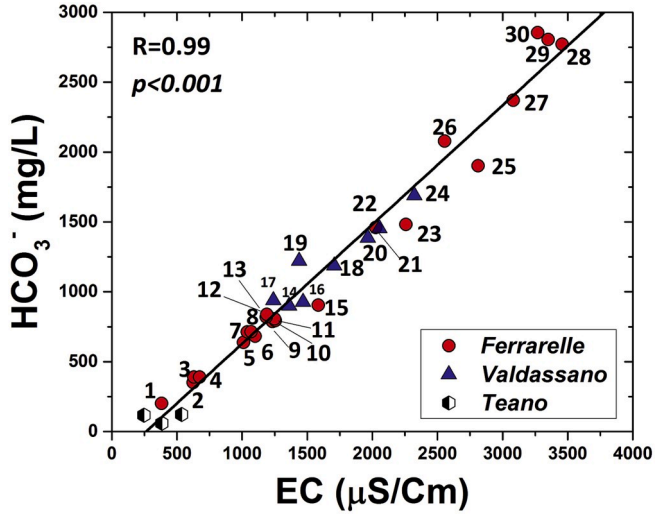


**Fig. 3.** A cross plot of bicarbonate concentration ([$HCO_3^-$]) and electrical conductivity (EC). Note that the dissolved $CO_2$ content and the degree of mineralization are highly correlated in groundwater samples from the current study areas.

enthalpy geothermal fluid circulation reported in Cuoco et al. (2017).

The K and As correlation (see Table 2) suggests that the chemical composition of $CO_2$-saturated Ferrarelle waters appear to be influenced by the ultra-potassic volcanic host rocks of Roccamonfina volcano, which agrees with previous studies from this region (Busico et al., 2020; Cuoco et al., 2010; Rouchon et al., 2008). Elevated levels of Fe, F, and Mg indicate that similar water-rock-gas interactions may influence more basic volcanics, such as basaltic water-rock interactions as has been suggested previously (Aiuppa et al., 2003; Brusca et al., 2001).

In addition to uncertainty in the type and degree of water-rock interactions at depth, the Eh conditions appear to vary with depth in this region. Note that the samples with the highest degree of mineralization (#28, #29, #30), which correspond to greatest sampling depths display reducing Eh values (Table 1). These trends are supported by field data that display moderate Eh (oxygen fugacity) at intermediate depths and increasing Eh in shallow waters within the volcanic sequences.

### 5.2. Tracing the inputs of $CO_2$

As noted above, $CO_2$ ($HCO_3^-$) levels are highly correlated to electrical conductivity and a variety geochemical proxies for extent of water-rock interactions. The correlation between $CO_2$ and electrical conductivity is consistent with the conservative mixing ('dilution') of over-pressured, $CO_2$-saturated waters with shallow fresh water. Isotopic tracers of water and gas can be useful for determining the source and interactions that occur by $CO_2$ interactions in the subsurface.

In the current study, we note significant linear correlations between $CO_2$ ($HCO_3^-$) and $\delta^{13}$C-DIC. The highly mineralized endmember documented in the current study has an upper limit of 4.1‰, while the $\delta^{13}$C-DIC values in the fresh water, $CO_2$-poor endmember is a low at −2.1‰. The dissolution of limestone typically produces $\delta^{13}C$–$CO_2$ that ranges from −1.0 to +2.0‰ (Craig, 1963; Darrah et al., 2013), whereas mantle-derived $CO_2$ typically ranges from −7.0 to −3.0‰ (Javoy et al., 1982; Rollinson, 1993). As a result, we conclude that samples that fall along Trend A in Fig. 6a that display low [$HCO_3^-$] are consistent with water-rock interactions with carbonate aquifers at the edges of the Riardo Plain (and potentially recharged along these units). However, simple one-stage water-rock interactions cannot explain the highly mineralized endmember.

The $\delta^{13}C$–$CO_2$ data in the gas emissions in the Roccamonfina area range between −2‰ and - 1‰ (Cuoco et al., 2017), suggesting $CO_2$ from

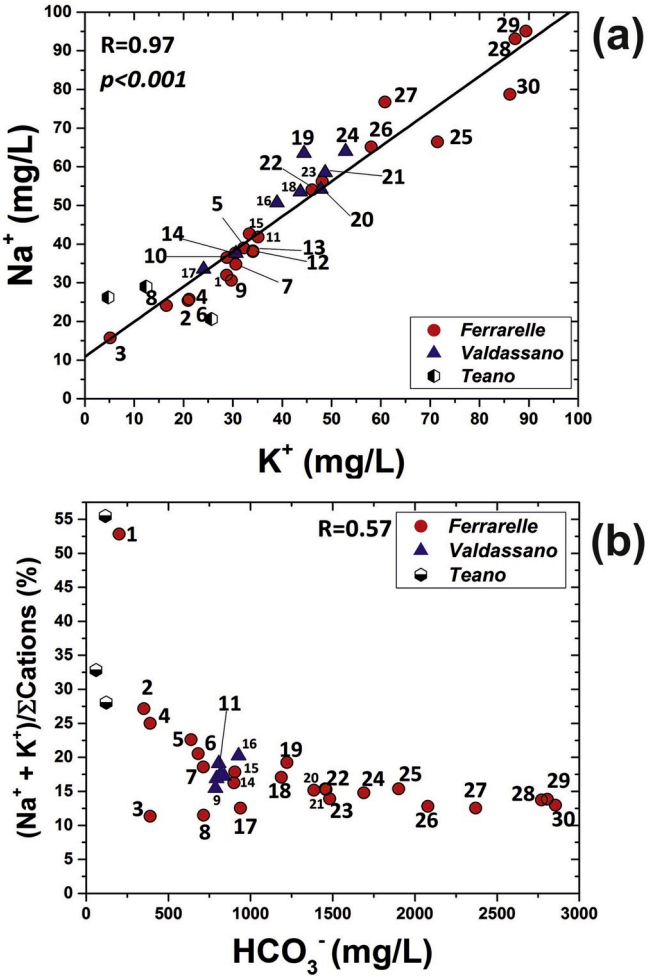


**Fig. 4.** A cross plot of sodium plus potassium ([$Na^+$] + [$K^+$] vs. [$HCO_3^-$] **(a)**, which plots along a exponential mixture between both components and **(b)** a cross plot of [$Na^+$] vs. [$K^+$]. Note that although the total concentration alkali elements increase with the degree of mineralization (i.e., highest $HCO_3^-$), the proportion of alkali content ($Na^+$ and $K^+$) actual decreases. Thus, with increasing mineralization, groundwater from the region becomes dominantly $Ca^{2+}$-$HCO_3$ type-waters and display total [$Na^+$ + $K^+$] of less than 20% of the cation abundance.

the system likely results from a mixture of carbonate rocks and mantle sources. The enrichment factor (ε) for chemical reactions at temperatures comparable with those of the investigated system is $\varepsilon^{13}C$–$CO_{2(g)}$-$CO_{2(sol)}$ ~ −1.1, while for $\varepsilon^{13}C$–$CO_{2(sol)}$-$HCO_3$ it is ~ +9 (Clark and Fritz, 1997). Therefore, a solution at equilibrium between $CO_2$ gas and water (dissolved inorganic carbon or DIC) should display a $\delta^{13}$C-DIC of about +6.4‰. From these assumptions, the $\delta^{13}$C-DIC values detected in our $CO_2$-saturated groundwater samples (Table 1) suggest that massive carbonate hydrolysis in the karst aquifer is required to lower the $\delta^{13}$C-DIC values to a range between 0‰ and +4‰. Most of the $CO_2$ and DIC-rich samples (e.g., samples #22, #25 in Fig. 6a) from the karst aquifer have $\delta^{13}$C-DIC values consistent with the isotopic processes proposed above.

The $\delta^{13}C$–$CO_2$ of the groundwater system appears to follow a 3-component mixing model with endmembers that include: (i) deep gas-saturated groundwater from the karstic carbonate basement (or even deeper); (ii) the groundwater hosted in the multilayered aquifer recharged only from the southeastern sector of Roccamonfina volcanics (e.g., #1); with minor contributions from (iii) shallow, fresh water recharged at higher elevation that interacts with local carbonate reliefs at the edge of the Riardo Plain (Fig. 1).

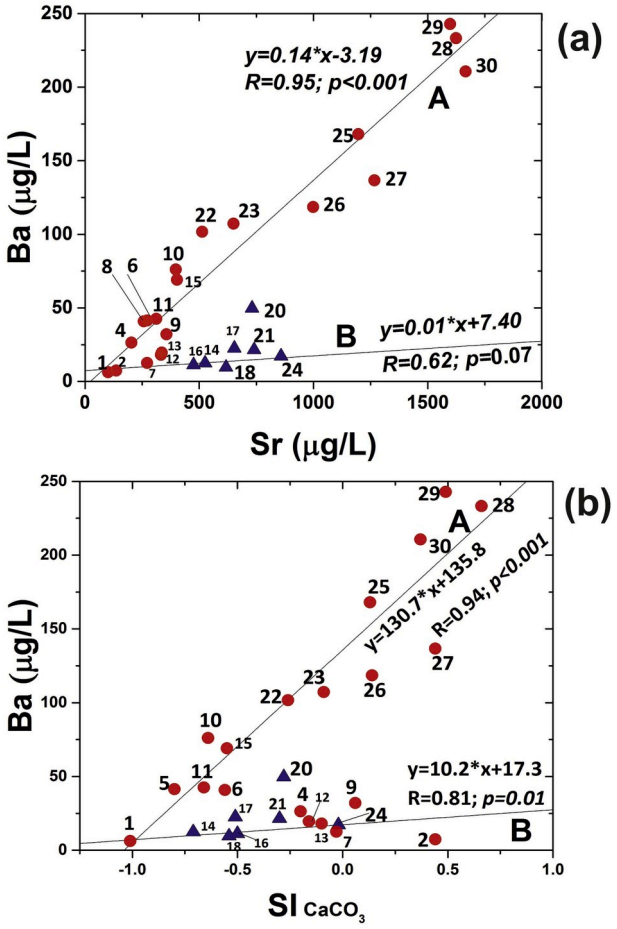


**Fig. 5.** A cross plot of [Ba] and [Sr] **(a),** and a cross plot of [Ba] and the calcite saturation index ($SI_{CaCO3}$) **(b)**. Note that both show two distinct trends, with the *Ferrarelle* and *Valdassano* samples following trends A and B, respectively.

Isotopes of water provide additional insight. We note a negative linear correlation between $\delta^{18}O$–$H_2O$ and $HCO_3^-$ and relatively low $\delta^{18}O$–$H_2O$ values throughout the study area. These data suggest that both potential recharge areas, including the Roccamonfina basal aquifer and the karst basement of the Riardo-Valdassano area, are likely located in an inland area at a higher topographic elevation (Minissale and Vaselli, 2011) than the current elevation of the Riardo Plain; this hypothesis is in agreement with the hydrogeological model by Viaroli et al. (2018). In this context, the $\delta^{18}O$–$H_2O$ data are useful for determining the recharge area, at least for samples with a low degree of mineralization (−6‰ to −5.8‰). The lower $\delta^{18}O$ values detected in the other samples with low degrees of mineralization (about −6.5‰) can be related to infiltration from elevations comparable with the southeastern slope of the Roccamonfina volcano or Mt. Coricuzzo (Mt Maggiore complex) (Fig. 1).

The significant correlation between $\delta^{18}O$–$H_2O$ and $\delta^{13}C$-DIC is interpreted as consistent with the mixing processes between the deep, $CO_2$-rich carbonate aquifer and the shallower, $CO_2$-poor aquifer hosted in the volcanic successions as described above. In fact, when other hydrogeochemical processes occur (e.g., mixing with shallow groundwater, changes of redox equilibria, and/or precipitation and adsorption), the correlation decreases. As a result, those waters affected by secondary geochemical processes potentially related to mixing of a third source of water in shallow aquifers (#5, #10, #12 and #15 in Fig. 6b and 6c), as inferred from geochemical data, appear to plot away from a simple two-component mixing line and have more scatter than the majority of the data, similar to what was observed for the fresher water samples in Fig. 6b and 6c.

The distribution of $^{222}Rn$, naturally produced by the radioactive decay of $^{238}U$, can provide useful clues about the mechanisms that influence mixing within this complex geological/hydrogeological structure. Waters hosted in the aquifer of the volcanic succession that likely recharged exclusively from the southeastern slope of the volcanic edifice (e.g., sample #1) have the highest Rn concentrations. In contrast, samples with significant contributions of fresher, younger water that likely recently recharged through shallow and less mineralized carbonate aquifers deviate from the main mixing line for many constituents, including Rn (Fig. 6d). These were likely sourced from the carbonate reliefs at the edge of the Riardo Plain and have not experienced any Rn contribution from volcanic successions. Initially, these trends may seem contrary to many other hydrological settings in which an increase in Rn would be expected with depth. However, in the Riardo Plain the shallow volcanic rocks overlay the carbonate basement and provide a shallower source of Rn into aquifers in this region (Tommasone et al., 2015, 2011; De Francesco et al., 2010a; b). Therefore, in this particular setting, Rn content in the water decreases as the proportion of $CO_2$ derived from the deep endmember increases.

Although we do not observe any linear correlations with Rn contents, we do observe elevated $^{222}Rn$ levels in samples collected from shallow depths, specifically Sample #1, that show high levels of $^{222}Rn$ and a high proportion of alkali elements. We do observe similar trends for $^{222}Rn$ and the percentage of alkali ions relative to [$HCO_3^-$] (Fig. 4b; 6 d). We anticipate that the Rn-rich waters that have interacted with local volcanic rocks are effectively diluted when vertical mixing introduces more deeply sourced, relatively Rn-poor, and $CO_2$/DIC-rich groundwater from the karstic basement following a history of gas-water-rock interactions (Fig. 6d). As a result, the groundwater upwelling from the carbonate basement along normal fault planes effectively dilutes the Rn content in the volcanic aquifer, while it quickly increases the DIC content.

### 5.3. Behavior of trace metals

The observed trace metal chemistry is consistent with this model and displays a decrease in the concentrations of Fe in solution with increasing Eh. In high Eh conditions, Fe forms Fe-oxyhydroxides, which precipitate within the aquifer. Although these were not directly observed in the current study, this hypothesis is consistent with lower levels of Fe in samples with elevated Eh. If verified, Fe-oxyhydroxide precipitation could account for the low levels of As, Ba, and other select metals in samples with low Fe. This hypothesis stems from the realization that Fe-oxyhydroxides have chemical structures compatible with a high ion adsorption capability that likely removes many metals (and cations more generally) by either co-precipitation with or adsorption onto the surfaces of the Fe oxyhydroxides (Hiemstra, 2013; Dzombak and Morel, 1990). Based on the inverse relationship between Ba (and As) and Eh (Table 2), Fe-oxyhydroxide precipitation provides a viable mechanism to explain the variations in water chemistry from the linear trends observed in highly mineralized waters.

The majority of data can be explained by simple 2-component mixing between a deep $CO_2$-rich water hosted in the carbonate basement and a shallow freshwater hosted in the volcanic successions. However, there are two sub-trends that suggest other factors also influence the composition of groundwater in the study area (Fig. 5). Overall, the data indicate that mixing processes presented as part of the *Ferrarelle* linear correlations dominate groundwater composition (sub-trend A, Fig. 5a), but that the composition of the *Valdassano* waters (sub-trend B, Fig. 5a) likely reflects dilution from an additional (third) source of water that is fresher, has higher oxygen fugacity (higher Eh), and is dominantly Ca–$HCO_3$ without influence of prior water-rock interactions with volcanic facies (Fig. 5b).

In order to better explain the observations from the Valdassano area, we developed a conceptual model to explain the hydrodynamic conditions that could account for water geochemistry from this area (Fig. 7).

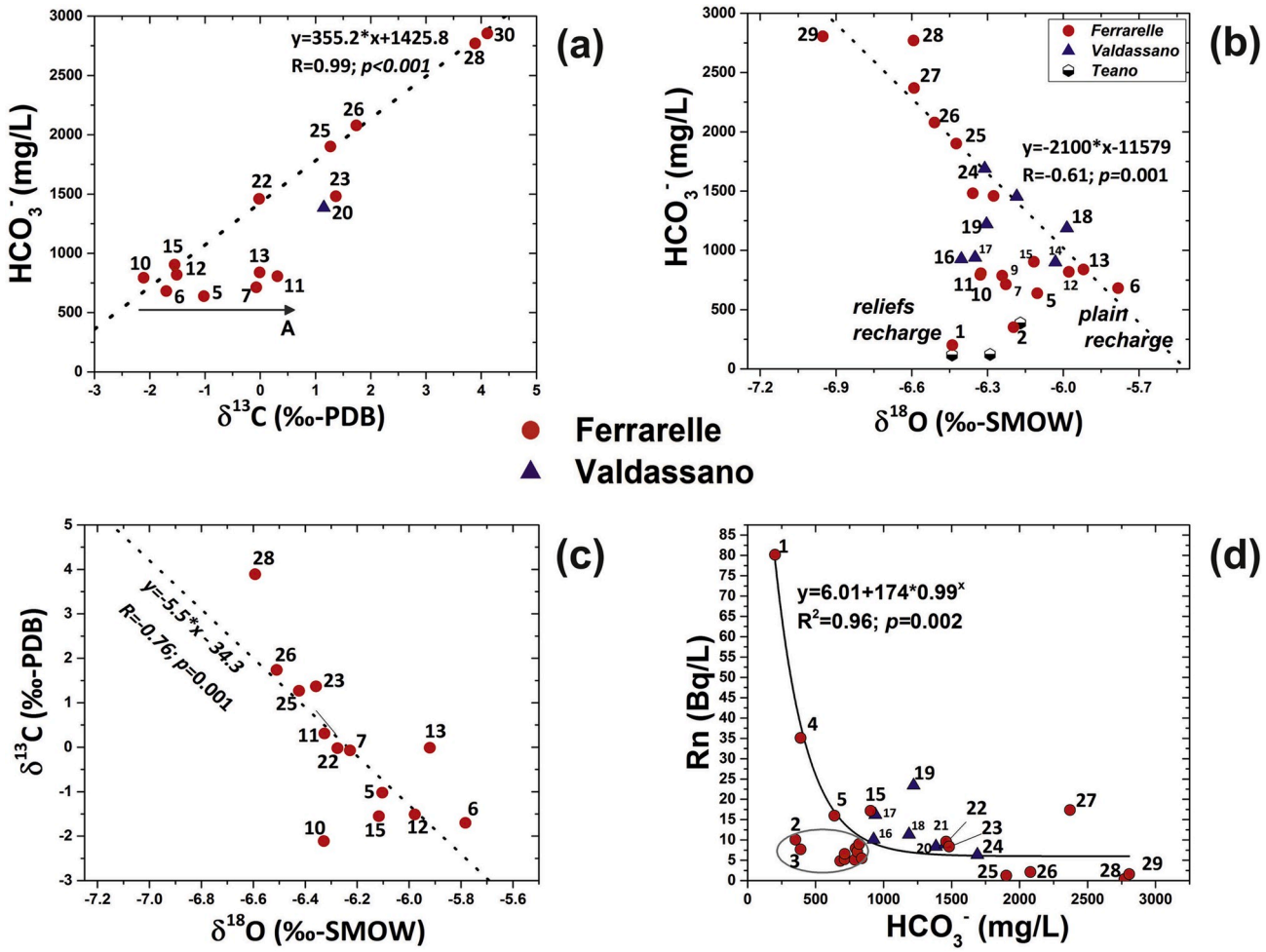


**Fig. 6.** Mixing processes detected through isotopic ($\delta^{18}O$, $\delta^{13}C$-DIC) and Rn concentration data. **(a)** $HCO_3^-$ vs. $\delta^{13}C$-DIC data suggest a gradual depletion in $^{13}C$-DIC of groundwater samples associated with upwelling of deep groundwater. Linear fit computed with N = 9 (#6, #10, #12, #15, #22, #25, #26, #28, #30) **(b)** The negative correlation between [$HCO_3^-$] and $\delta^{18}O$–$H_2O$ suggests that the gas saturated groundwater is recharged by local rainfall. Samples with [$HCO_3^-$] lower than 1000 mg/L that deviate from the best fit line exhibit more negative $\delta^{18}O$–$H_2O$ values (−6.4 and −6.0‰) due to the higher recharge elevations (with respect to the Riardo plain); **(c)** The $\delta^{18}O$–$H_2O$ - $\delta^{13}C$-DIC correlation supports the proposed dominantly 2-component mixing model; and **(d)** When compared to $HCO_3^-$, Rn mobilization follows a exponential function reflecting mixing of waters with varying concentrations.

The tendency of Eh to decrease with an increasing calcite saturation index ($SI_{CaCO3}$) is consistent with the additional mixture with $O_2$ and Ca–$HCO_3$-rich waters. We hypothesize that the freshwater recharge that contributes to the best-fit trend depicted as sub-trend B likely originates in the region where the contiguous carbonate units outcrop near Mt. Coricuzzo. These observations agree with other recent hydrogeological investigations in the region (e.g., Mazza et al., 2013). In this scenario, the addition of oxygen-rich water could mix and establish a new chemical equilibrium for groundwater in the region (*Ferrarelle*-type water). The oxygen-rich waters could be the contributions that mix with and catalyze Fe oxyhydroxide precipitation which adsorbs Ba, hence removing dissolved metals from the water solution (see "B trends" in Fig. 5).

The chemical composition of the poorly mineralized shallow groundwater of the Riardo Plain is similar to that of the local shallow aquifer of the volcanic succession along the southeastern slope of the Roccamonfina Volcano (i.e., the *Teano* samples). Local increases in $NO_3^-$ and $SO_4^{2-}$ in this area have been attributed to human activities (Busico et al., 2018; Cuoco et al., 2015). Unlike $NO_3^-$ and $SO_4^{2-}$, elevated levels of vanadium (V) appears to be a natural tracer of geogenic water-rock interactions. Vanadium can be enriched in volcanic aquifers by water-rock interactions with pyroclastic rocks (Rango et al., 2013). Specifically within shallow, oxidizing, and circum-neutral groundwater conditions, V can be used to track water-rock interactions with volcanic sediments (Wehrli and Stumm, 1989).

### 5.4. Geochemical modeling of the mineralization process

The processes leading to the formation of the highly mineralized, $CO_2$-rich endmember described above were investigated with a forward geochemical model simulating the geochemical evolution of groundwater subjected to an input of $CO_{2(g)}$ and dissolvable mineral phases (Nordstrom and Campbell, 2014). Sample #3, which represents groundwater circulating within the carbonate aquifer and displays both low mineralization and low element content, was assumed to represent the starting fluid composition in the forward geochemical model. The elements used in the geochemical model include Ca, Mg, Na, K, C(IV), and Cl. The phases entering the solution were selected based on the following observations:

a) [$Ca^{2+}$] + [$Mg^{2+}$] shows a 1:2 M ratio with $HCO_3^-$, and samples are all of Ca–$HCO_3$ type (with the exception of sample #1, of Ca–Na–$HCO_3$ type). Therefore, the dissolution of carbonates is mostly responsible for the observed increase in mineral contents;

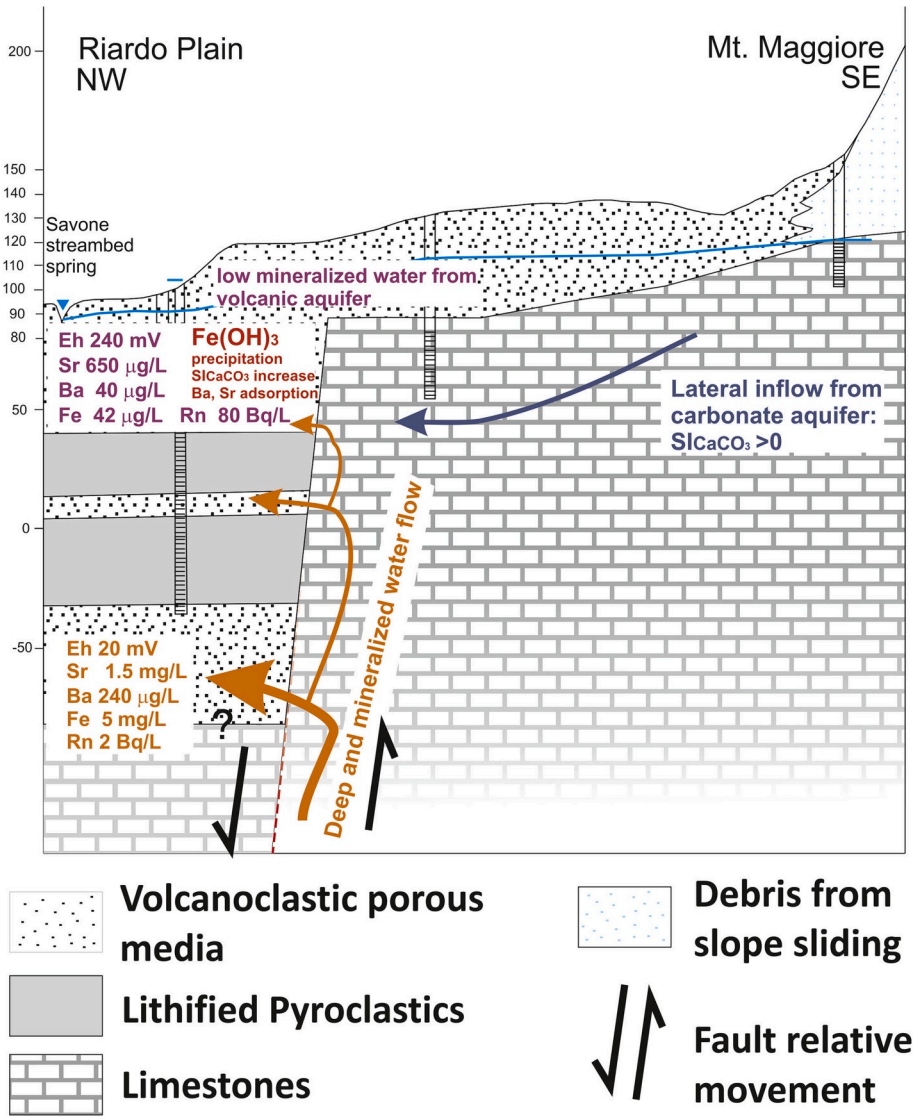


**Fig. 7.** Conceptual model of mixing dynamics occurring in the Valdassano shallow aquifer. A lateral recharge from Mt. Coricuzzo adds a third endmember to the vertical mixing (deep vs. shallow groundwater). As a result, a specific hydrogeochemical equilibrium is detected in the Valdassano area and near the base of Mt. Coricuzzo, which can be observed through the adsorption of alkali earth trace elements (e.g., Ba and Sr) onto the Fe-oxyhydroxides as a result of a recent increase in oxygen fugacity.

b) $[Cl^-]$ is also significantly correlated to the $HCO_3^-$ content and could derive from halite or from fluid inclusions trapped in the carbonate formations;
c) $[Na^+]$ and $[K^+]$ are largely in excess with respect to $[Cl^-]$. Since their relative content is higher in samples with low degrees of mineralization circulating in the volcanic aquifers, they could be derived from the dissolution of silicates or volcanic glass.

Therefore in the forward geochemical model we assumed that the groundwater pH, which likely varies as a function of the strong input of $CO_{2(g)}$, would promote the dissolution of calcite, dolomite, and halite from the carbonate aquifer, and the dissolution of silicates such as albite and K-feldspar from the volcanic formations (Conticelli et al., 2009). The relative amounts of each mineral phase were calculated by mass balance, using the difference in composition between sample #28 (representative of the mineralized, $CO_2$-rich endmember) and sample #3 (the shallower, $CO_2$-poor endmember). Sulfate was not selected as a constraint because its concentration in the mineralized endmember, due to its lower redox potential, was lower than in the starting solution.

The model values obtained are:

Initial water + 0.0686 $CO_{2(g)}$ + 0.0129 calcite + 0.00182 dolomite + 0.00024 halite + 0.00313 albite + 0.00211 K-feldspar → Final waterwhere the amounts of each mineral phase are given in moles per L of solution.

Table 3 reports the comparison between the model output and sample #28, for selected parameters calculated by the software based on ionic mass balance (pH and EC) and speciation. The comparison is within 3% error for most parameters, and about 5% for the concentration of $HCO_3^-$ and $SI_{CaCO3}$.

The model indicates that 3,020 mg of $CO_2$ is dissolved per L of water, which produces a final solution that is saturated in $CO_2$ ($SI_{CO2} = 0.03$) with a total C(IV) of 0.093 mol/L (1,116 mg/L), of which about 0.044 mol/L (2,688 mg/L) as $HCO_3^-$ and about 0.045 mol/L (1,980 mg/L) as $CO_2$. The model accurately reproduces the chemical composition of the mineralized endmember of the mixing process observed in the Riardo Plain waters, and further supports the conclusion that this groundwater

**Table 3**
Results of the geochemical model in comparison with the highly mineralized $CO_2$-rich endmember.

| Parameter (unit) | Sample #3 | Model output | Sample #28 | % error |
|---|---|---|---|---|
| EC (µS/cm) | 566 | 2882 | 2968 | −2.90 |
| pH | 7.80 | 6.30 | 6.24 | 0.96 |
| $SI_{CaCO3}$ | 0.04 | 0.69 | 0.66 | 4.54 |
| log $pCO_2$ (molar) | −2.84 | −1.34 | −1.32 | 1.51 |
| $HCO_3^-$ (mg/L) | 389.5 | 2688 | 2771 | −2.98 |

contains elements derived from both volcanic sediments and carbonates. However, considering that this water is naturally sparkling and supersaturated with respect to calcite, some dissolved $CO_2$ could be lost during the upwelling of the solution in the conductive fractures. The model is also in agreement with evidence from $\delta^{13}$C-DIC values, suggesting that the acidification caused by the deep $CO_2$ input is buffered by the dissolution of the carbonate host rock, as commonly observed in natural analogue and geochemical modelling studies (e.g., Kharaka et al., 2006; Keating et al., 2009).

## 6. Conclusions

The Ferrarelle aquifer system is a multilayer aquifer encompassing a deep, karstic aquifer confined within a carbonate basement that interacts with other aquifers hosted in shallower volcanic successions. Chemical and isotopic data suggest that groundwater hosted in the shallower volcanic aquifers that displays a low degree of mineralization is recharged from: i) the southeastern slope of Roccamonfina, ii) the shallow aquifer of the Riardo Plain and, likely, in some cases iii) Mt. Coricuzzo, located in the Valdassano area. In line with previous investigations, groundwater hosted in the deep Ferrarelle carbonate basement is laterally recharged by water flowing from the Roccamonfina volcano, which intercepts the deep gas circulation and migrates vertically under natural pressure gradients along the SW-NE trending normal faults present in the Riardo Plain. Along this flowpath, groundwater mixes with poorly mineralized water hosted in the upper volcanic succession. The deep mineralized groundwater is enriched in elements derived from both volcanics and carbonates due to gas-water-rock interactions along the groundwater flowpath. Positive correlations ($R > 0.8$) among all conservative elements in solution points to dominantly two-component mixing of deep, gas-saturated waters hosted in the upper carbonatic layers and shallow waters hosted in local volcanics. The dominantly vertical mixing produces strong correlations of conservative elements as evidenced by their linear fits. Other hydrogeological processes (e.g., mixing with a third oxygen-rich endmember) can locally alter the geochemical trends catalyzed by vertical mixing and lead to deviations of chemical compositions from the dominantly two-component mixing pattern. Examples of these deviations include samples from the Valdassano aquifer, in which oxygen input from fresh waters causes an increase of Eh and the precipitation of Fe oxy-hydroxides along with adsorbed elements (e.g., Ba, As), which produce a secondary trend deviating from the main trend on the correlation plot.

The forward geochemical model indicates that at temperatures as low as those present in the Ferrarelle aquifer, influence discharges of geogenic $CO_2$ that reach (and exceed) saturation levels in deep aquifers. The model suggests that the amount of dissolved $CO_2$ is almost 3 g/L, in agreement with direct measurements (pH, $HCO_3^-$). Mixing allows partial loss of the $CO_2$ load, which has been confirmed by multiple observations of visible bubbling/degassing. On the other hand, freshwater samples with low degrees of mineralization display more depleted $\delta^{13}$C-DIC from atmospheric/groundwater equilibrium and groundwater/carbonate equilibrium. As a result, robust interpretations require the adequate characterization of various geochemical components and should not rely on a single tracer alone (e.g., $\delta^{13}$C-DIC in the absence of [$HCO_3^-$]).

The observed radon content follows a exponential function with all the conservative ions in solution. This function explains the mixing dynamics between a deep Rn-poor carbonate endmember with a shallow Rn-richer volcanic aquifer. The statistical correlations among these chemical variables can be used to quantify the leakage of $CO_2$ into the aquifer connected with the gas-saturated reservoir through local faults. In conclusion, we are able to trace $CO_2$-leakage processes and pathways in freshwater aquifers connected with natural or anthropogenic gas-saturated reservoirs using a suite of geochemical tracers. The overall hydrodynamic setting of the Riardo Plain provides a natural laboratory for the investigation of geochemical processes involved in the mixing of migrating $CO_2$ or a $CO_2$-influenced groundwater.

## Declaration of competing interest

The authors declare that they have no known competing financial interests or personal relationships that could have appeared to influence the work reported in this paper.

## Acknowledgements

The authors would thank Ferrarelle joint stock company for the collaboration and founding in the research projects on Riardo Plain hydrogeologic system. The authors want also thank all the anonymous referees which with their comments have allowed the improvement of the quality of the manuscript.

## References

Aiuppa, A., Bellomo, S., Brusca, L., D'Alessandro, W., Federico, C., 2003. Natural and anthropogenic factors affecting groundwater quality of an active volcano (Mt. Etna, Italy). Appl. Geochem. 18 (6), 863–882. https://doi.org/10.1016/S0883-2927(02)00182-8.

Amonette, J.E., Zhong, L., Darrah, T.H., Grove, B.S., Cole, D.R., 2019. Noble and major gases released from rock core materials as intrinsic tracers for detecting carbon dioxide leakage–Laboratory evaluation. Int. J.Greenh.Gas Control 89, 76–88.

Bense, V.F., Gleeson, T., Loveless, S.E., Bour, O., Scibek, J., 2013. Fault zone hydrogeology. Earth Sci. Rev. 127, 171–192. https://doi.org/10.1111/gfl.12205.

Brunetti, E., Jones, J.P., Petitta, M., Rudolph, D.L., 2013. Assessing the impact of large-scale dewatering on fault-controlled aquifer systems: a case study in the Acque Albule basin (Tivoli, central Italy) [Evaluation de l'impact d'un dénoyage à grande échelle de systèmes aquifères contrôlés par faille: Le cas d'étude du Bassin d'Acque Albule (Tivoli, Italia centrale). Hydrogeol. J. 21 (2), 401–423. https://doi.org/10.1007/s10040-012-0918-3.

Brusca, L., Aiuppa, A., D'Alessandro, W., Parello, F., Allard, P., Michel, A., 2001. Geochemical mapping of magmatic gas-water-rock interactions in the aquifer of Mount Etna volcano. J. Volcanol. Geoth. Res. 108 (1–4), 199–218. https://doi.org/10.1016/S0377-0273(00)00286-9.

Busico, G., Kazakis, N., Cuoco, E., Colombani, N., Tedesco, D., Voudouris, K., Mastrocicco, M., 2020. A novel hybrid method of specific vulnerability to anthropogenic pollution using multivariate statistical and regression analyses. Water Res. 171.

Busico, G., Cuoco, E., Kazakis, N., Colombani, N., Mastrocicco, M., Tedesco, D., Voudouris, K., 2018. Multivariate statistical analysis to characterize/discriminate between anthropogenic and geogenic trace elements occurrence in the Campania Plain. South.Italy.Environ. Pollut. 234, 260–269. https://doi.org/10.1016/j.envpol.2017.11.053.

Chen, M., Buscheck, T.A., Wagoner, J.L., Sun, Y., White, J.A., Chiaramonte, L., Aines, R. D., 2013. Analysis of fault leakage from Leroy underground natural gas storage facility, Wyoming, USA [Analyse d'une fuite par faille de l'installation de stockage souterrain de gaz naturel de Leroy, Wyoming, USA] Hydrogeology. J. 21 (7), 1429–1445. https://doi.org/10.1007/s10040-013-1020-1.

Clark, I.D., Fritz, P., 1997. Environmental Isotopes in Hydrogeology. CRC Press/Lewis Publishers, Boca Raton, FL.

Craig, H., 1963. The isotopic geochemistry of water and carbon in geothermal areas. In: Tongiorgi, E. (Ed.), Nuclear Geology on Geothermal Areas. CNR. Italian Council for Research), Spoleto, Italy, pp. 17–54.

Conticelli, S., Marchionni, S., Rosa, D., Giorando, G., Boari, E., Avanzinelli, R., 2009. Shoshonite and sub-alkaline magmas from an ultrapotassic volcano: Sr–Nd–Pb isotope data on Roccamonfina volcanic rocks, Roman Magmatic province, Southern Italy. Contrib. Mineral. Petrol. 157, 41–63. https://doi.org/10.1007/s00410-008-0319-8.

Cuoco, E., Minissale, A., Di Leo, A., Tamburrino, S., Iorio, M., Tedesco, D., 2017. Fluid geochemistry of the Mondragone hydrothermal systems (southern Italy): water and gas compositions vs. geostructural setting. Int. J. Earth Sci. 106 (7), 2429–2444. https://doi.org/10.1007/s00531-016-1439-4.

Cuoco, E., Darrah, T.H., Buono, G., Verrengia, G., De Francesco, S., Eymold, W.K., Tedesco, D., 2015. Inorganic contaminants from diffuse pollution in shallow groundwater of the Campanian Plain (Southern Italy). Implications for geochemical survey. Environ. Monit. Assess. 187 (2), 46. https://doi.org/10.1007/s10661-015-4307-y.

Cuoco, E., Spagnuolo, A., Balagizi, C., De Francesco, S., Tassi, F., Vaselli, O., Tedesco, D., 2013. Impact of volcanic emissions on rainwater chemistry: the case of Mt. Nyiragongo in the Virunga volcanic region (DRC). J. Geochem. Explor. 125, 69–79. https://doi.org/10.1016/j.gexplo.2012.11.008.

Cuoco, E., Verrengia, G., De Francesco, S., Tedesco, D., 2010. Hydrogeochemistry of Roccamonfina Volcano (southern Italy). Environmental Earth Sciences 61 (3), 525–538. https://doi.org/10.1007/s12665-009-0363-3.

Darrah, T.H., Jackson, R.B., Vengosh, A., Warner, N.R., Whyte, C.J., Walsh, T.B., Kondash, A.J., Poreda, R.J., 2015. The evolution of Devonian hydrocarbon gases in shallow aquifers of the northern Appalachian Basin: insights from integrating noble gas and hydrocarbon geochemistry. Geochem. Cosmochim. Acta 170, 321–355.

Darrah, T.H., Tedesco, D., Tassi, F., Vaselli, O., Cuoco, E., Poreda, R.J., 2013. Gas chemistry of the dallol region of the danakil depression in the Afar region of the northern-most east african rift. Chem. Geol. 339, 16–29.
De Francesco, S., Tommasone, F.P., Cuoco, E., Tedesco, D., 2010a. a. Indoor radon seasonal variability at different floors of buildings. Radiat. Meas. 45 (8), 928–934. https://doi.org/10.1016/j.radmeas.2010.05.026.
De Francesco, S., Tommasone, F.P., Cuoco, E., Verrengia, G., Tedesco, D., 2010b. b. Radon hazard in shallow groundwaters: amplification and long-term variability induced by rainfall. Sci. Total Environ. 408 (4), 779–789. https://doi.org/10.1016/j.scitotenv.2011.05.039.
De Rita, D., Giordano, G., 1996. Volcanological and structural evolution of Roccamonfina volcano (Italy): origin of the summit caldera. Geol. Soc. Spec. Publ. 110, 209–224. https://doi.org/10.1144/GSL.SP.1996.110.01.16 (Volcano Instability on Earth and Other Planets).
De Vivo, B., Rolandi, G., Gans, P.B., Calvert, A., Bohrson, W.A., Spera, F.J., Belkin, H.E., 2001. New constraints on the pyroclastic eruptive history of the Campanian volcanic Plain (Italy). Mineral. Petrol. 73 (1–3), 47–65. https://doi.org/10.1007/s007100170010.
Dzombak, D., Morel, F., 1990. Surface Complexation Modeling: Hydrous Ferric Oxide. Wiley, New York, p. 393.
Drever, J., 1997. The Geochemistry of Natural Waters. Prentice Hall, New Jersey.
Epstein, S., Mayeda, T.K., 1953. Variation of the $^{18}O/^{16}O$ ratio in natural waters. Geochem. Cosmochim. Acta 4, 213–224. https://doi.org/10.1016/0016-7037(53)90051-9.
Eymold, W.K., Swana, K., Moore, M.T., Whyte, C.J., Harkness, J.S., Talma, S., Murray, R., Moortgat, J.B., Miller, J., Vengosh, A., Darrah, T.H., 2018. Hydrocarbon-rich groundwater above shale-gas formations: a karoo basin case study. Groundwater 56 (2), 204–224.
Giannetti, B., 2001. Origin of the calderas and evolution of Roccamonfina volcano (Roman region, Italy). J. Volcanol. Geoth. Res. 106, 301–319. https://doi.org/10.1016/S0377-0273(00)00259-6.
Giannetti, B., Luhr, J.F., 1983. The white trachytic Tuff of Roccamonfina Volcano (roman region, Italy). Contrib. Mineral. Petrol. 84, 235–252. https://doi.org/10.1007/BF00371289.
Giordano, G., Naso, G., Scrocca, D., Funiciello, R., Catalani, F., 1995. Processi di estensione e circolazione di fluidi a Bassa termalità nella Piana di Riardo (Caserta, Appennino Centro-Meridionale). Boll. Soc. Geol. Ital. 114, 361–371.
Glennon, J.A., Pfaff, R.M., 2005. The operation and geography of carbon-dioxide-driven, cold-water geysers. GOSA Transactions 9, 184–192.
Harkness, J.S., Swana, K., Eymold, W.K., Miller, J., Murray, R., Talma, S., Whyte, C.J., Moore, M.T., Maletic, E.L., Vengosh, A., Darrah, T.H., 2018. Pre-drill groundwater geochemistry in the Karoo Basin, South Africa. Groundwater 56 (2), 187–203.
Hiemstra, T., 2013. Surface and mineral structure of ferrihydrite. Geochem. Cosmochim. Acta 105, 316–325. https://doi.org/10.1039/c7en01060e.
Javoy, M., Pineau, F., Allegre, C.J., 1982. Carbon geodynamic cycle. Nature 300, 171–173.
Keating, E.H., Fessenden, J., Kanjorski, N., Koning, D.J., Pawar, R., 2009. The impact of $CO_2$ on shallow groundwater chemistry: observations at a natural analog site and implications for carbon sequestration. Environmental Earth Sciences 60, 521–536. https://doi.org/10.1007/s12665-009-0192-4.
Kharaka, Y.K., Thordsen, J.J., Hovorka, S.D., Seay Nance, H., Cole, D.R., Phelps, T.J., Knauss, K.G., 2009. Potential environmental issues of $CO_2$ storage in deep saline aquifers: geochemical results from the frio-I brine pilot test, Texas, USA. Appl. Geochem. 24 (6), 1106–1112. https://doi.org/10.1016/j.apgeochem.2009.02.010.
Kharaka, Y.K., Cole, D.R., Thordsen, J.J., Kakouros, E., Nance, H.S., 2006. Gas-water-rock interactions in sedimentary basins: $CO_2$ sequestration in the frio formation, Texas, USA. J. Geochem. Explor. 89 (1–3), 183–186. https://doi.org/10.1130/G22357.1. SPEC. ISS.
Kreuzer, R.L., Darrah, T.H., Grove, B.S., Moore, M.T., Warner, N.R., Eymold, W.K., Whyte, C.J., Mitra, G., Jackson, R.B., Vengosh, A., Poreda, R.J., 2018. Structural and hydrogeological controls on hydrocarbon and brine migration into drinking water aquifers in southern New York. Groundwater 56 (2), 225–244.
Langmuir, D., 1997. Aqueous Environmental Geochemistry. Prentice-Hall, Inc., Upper Saddle River, New Jersey.
Lawter, A.R., Qafoku, N.P., Asmussen, R.M., Kukkadapu, R.K., Qafoku, O., Bacon, D.H., Brown, C.F., 2018. Element mobilization and immobilization from carbonate rocks between $CO_2$ storage reservoirs and the overlying aquifers during a potential $CO_2$ leakage. Chemosphere 197, 399–410. https://doi.org/10.1016/j.chemosphere.2017.12.199.
Lu, X., Watson, A., Gorin, A.V., Deans, J., 2005. Measurements in a low temperature $CO_2$-driven geysering well, viewed in relation to natural geysers. Geothermics 34 (4), 389–410. https://doi.org/10.1016/j.geothermics.2005.05.001.
Luhr, J.F., Giannetti, B., 1987. The Brown Leucitic Tuff of Roccamonfina Volcano (roman region, Italy). Contributions to Mineralogy and Petrography 95, 420–436. https://doi.org/10.1007/BF00402203.
Mazza, R., Pietrosante, A., Taviani, S., Viaroli, S., 2013. A preliminary understanding of groundwater exchanges between the Riardo Plain and Mount Maggiore ridge (Campania, Italy). Rendiconti Online Societa Geologica Italiana 24, 207–209.
Minissale, A., Vaselli, O., 2011. Karst springs as "natural" pluviometers: constraints on the isotopic composition of rainfall in the Apennines of central Italy. Appl. Geochem. 26 (5), 838–852. https://doi.org/10.1016/j.apgeochem.2011.02.005.
Minissale, A., 2004. Origin, transport and discharge of $CO_2$ in central Italy. Earth Sci. Rev. 66 (1–2), 89–141. https://doi.org/10.1016/j.earscirev.2003.09.001.
Nisi, B., Vaselli, O., Elio, J., Giannini, L., Tassi, F., Guidi, M., Darrah, T.H., Maletic, E.L., Delgado Huertas, A., Marchionni, S., 2019. The campo de Calatrava volcanic field (central Spain): fluid geochemistry in a CO2-rich area. Appl. Geochem. 102, 153–170.
Nordstrom, D.K., Campbell, K.M., 2014. Modeling low-temperature geochemical processes In: Treatise on Geochemistry, second ed., vol. 7, pp. 27–68. https://doi.org/10.1016/B978-0-08-095975-7.00502-7
Parkhurst, D.L., Appelo, C.A.J., 1999. User's guide to PHREEQC (Version 2) - a computer program for speciation, batch-reaction, one-dimensional transport, and inverse geochemical calculations. U.S. Geological Survey Water-Resources Investigations Report 99–4259, 310.
Patacca, E., Scandone, P., 2007. Geology of the southern apennines. Bollettino della Società geologica italiana. Ital. J.Geosci. 7, 75–119.
Rango, T., Vengosh, A., Dwyer, G., Bianchini, G., 2013. Mobilization of arsenic and other naturally occurring contaminants in groundwater of the main Ethiopian rift aquifers. Water Res. 47 (15), 5801–5818. https://doi.org/10.1016/j.watres.2013.07.002.
Rollinson, H., 1993. Using Geochemical Data. Longman Group, London (UK).
Rouchon, V., Gillot, P.Y., Quidelleur, X., Chiesa, S., Floris, B., 2008. Temporal evolution of the Roccamonfina volcanic complex (Pleistocene), Central Italy. J. Volcanol. Geoth. Res. 177 (2), 500–514. https://doi.org/10.1016/j.jvolgeores.2008.07.016.
Ryan, P.C., 2014. Environmental and Low Temperature Geochemistry. Wiley-Blackwell, Chichester, West Sussex; Hoboken, NJ.
Shaffer, G., 2010. Long-term effectiveness and consequences of carbon dioxide sequestration. Nat. Geosci. 3 (7), 464–467.
Siller, A., Hofmann, H., Underschultz, J., Baublys, K., Hudson, N., 2018. Fractionation processes of $\delta^{13}C$ in a soil-shallow groundwater system of a potential $CO_2$ sequestration site: wandoan, QLD, Australia. Appl. Geochem. 96, 191–203. https://doi.org/10.1016/j.apgeochem.2018.06.009.
Stumm, W., Morgan, J.J., 1996. Aquatic Chemistry: Chemical Equilibria and Rates in Natural Waters. Wiley-Interscience publication. https://trove.nla.gov.au/work/31691612.
Szulczewski, M.L., MacMinn, C.W., Herzog, H.J., Juanes, R., 2012. Lifetime of carbon capture and storage as a climate-change mitigation technology. Proc. Natl. Acad. Sci. Unit. States Am. 109 (14), 5185–5189.
Takaya, Y., Nakamura, K., Kato, Y., 2018. Long-term reaction characteristics of $CO_2$–Water–Rock interaction: insight into the potential groundwater contamination risk from underground $CO_2$ storage. Resour. Geol. 68 (1), 93–100. https://doi.org/10.1111/rge.12147.
Tommasone, F.P., De Francesco, S., Carbone, P., Cuoco, E., Tedesco, D., 2015. Rainstorm induced soil $^{222}Rn$ concentration spikes observed in Southern Italy. Environmental Earth Sciences 73 (12), 8177–8187. https://doi.org/10.1007/s12665-014-3976-0.
Tommasone, F.P., De Francesco, S., Cuoco, E., Verrengia, G., Santoro, D., Tedesco, D., 2011. Radon hazard in shallow groundwaters II: dry season fracture drainage and alluvial fan upwelling. Sci. Total Environ. 409 (18), 3352–3363. https://doi.org/10.1016/j.scitotenv.2011.05.039.
USGS, 2011. National Field Manual for the Collection of Water-Quality Data. US Geological Survey, Washington, DC.
Viaroli, S., Lotti, F., Mastrorillo, L., Paolucci, V., Mazza, R., 2019. Simplified two-dimensional modelling to constrain the deep groundwater contribution in a complex mineral water mixing area, Riardo plain, southern Italy. Hydrogeol. J. https://doi.org/10.1007/s10040-018-1910-3 (in press).
Viaroli, S., Mastrolillo, L., Lotti, F., Paolucci, V., Mazza, R., 2018. The groundwater budget: a tool for preliminary estimation of the hydraulic connection between neighboring aquifers. J. Hydrol. 556, 72–86. https://doi.org/10.1016/j.jhydrol.2017.10.066.
Viaroli, S., Cuoco, E., Mazza, R., Tedesco, D., 2016. Dynamics of natural contamination by aluminium and iron rich colloids in the volcanic aquifers of Central Italy. Environ. Sci. Pollut. Control Ser. 23 (19), 19958–19977. https://doi.org/10.1007/s11356-016-7198-8.
Wehrli, B., Stumm, W., 1989. Vanadyl in natural waters: adsorption and hydrolysis promote oxygenation. Geochem. Cosmochim. Acta 53, 69–77. https://doi.org/10.1016/0016-7037(89)90273-1.
Wendlandt, R.F., Eggler, D.H., 1980. The origin of potassic magmas. Melting relations in the system $KAlSiO_4$–$Mg_2SiO_4$–$SiO_2$ and $KAlSiO_4$–MgO–$SiO_2$–$CO_2$ to 30 kilobars. Am. J. Sci. 280, 385–420.
Xu, T., Kharaka, Y.K., Doughty, C., Freifeld, B.M., Daley, T.M., 2010. Reactive transport modeling to study changes in water chemistry induced by $CO_2$ injection at the frio-I brine pilot. Chem. Geol. 271 (3–4), 153–164. https://doi.org/10.1016/j.chemgeo.2010.01.006.